

On the Progenitor of the Type IIb Supernova 2016gkg

Charles D. Kilpatrick^{1*}, Ryan J. Foley¹, Louis E. Abramson², Yen-Chen Pan¹,
Cicero-Xinyu Lu², Peter Williams², Tommaso Treu², Matthew R. Siebert¹,
Christopher D. Fassnacht³, Claire E. Max¹

¹*Department of Astronomy and Astrophysics, University of California, Santa Cruz, CA 95064, USA*

²*Department of Physics and Astronomy, University of California, Los Angeles, CA 90095, USA*

³*Department of Physics, University of California, One Shields Avenue, Davis, CA 95616, USA*

Accepted 0000, Received 0000, in original form 0000

ABSTRACT

We present a detection in pre-explosion *Hubble Space Telescope* (*HST*) imaging of a point source consistent with being the progenitor star of the Type IIb supernova (SN IIb) 2016gkg. Post-explosion imaging from the Keck Adaptive Optics system was used to perform relative astrometry between the Keck and *HST* imaging. We identify a single point source in the *HST* images coincident with the SN position to $0.89\text{-}\sigma$. The *HST* photometry is consistent with the progenitor star being an A0Ia star with $T = 9500\text{ K}$ and $\log(L/L_{\odot}) = 5.15$. We find that the SN 2016gkg progenitor star appears more consistent with binary than single-star evolutionary models. In addition, early-time light curve data from SN 2016gkg revealed a rapid rise in luminosity within ~ 0.4 days of non-detection limits, consistent with models of the cooling phase after shock break-out. We use these data to determine an explosion date of 20.15 September 2016 and progenitor star radius of $\log(R/R_{\odot}) = 2.41$, which agrees with photometry from the progenitor star. Our findings are also consistent with detections of other SNe IIb progenitor stars, although more luminous and bluer than most other examples.

Key words: stars: evolution — supernovae: general — supernovae: individual (SN 2016gkg)

1 INTRODUCTION

Any normal core-collapse supernova (CCSN) can yield valuable new insight into SN explosion mechanisms when its progenitor star is detected in pre-explosion imaging. The two canonical examples are SNe 1987A and 1993J, which revealed, among other aspects of SNe and their progenitor stars, that binary evolution is central to SNe (Aldering et al. 1994), that stars in the mass range $15\text{--}25\ M_{\odot}$ explode as SNe (Arnett et al. 1989; Podsiadlowski 1993; Maund et al. 2004), and that mass-transfer can describe both the hydrogen envelopes and circumstellar environments of some SNe (e.g., Weiler et al. 2007; Morris & Podsiadlowski 2007). Beyond these well-studied examples, roughly 20 progenitor systems have been identified and statistical studies of the connection between progenitor stars and SNe are now possible (Smartt et al. 2009; Smartt 2015). Of particular interest is the luminosity and colour distribution of these progenitor stars and inferences about their physical properties. Apart from notable examples such as SN 1987A and SN 2009ip (Arnett 1987; Woosley et al. 1987; Mauerhan et al. 2013), virtually all SN progenitor stars have $B - V > 0.3\text{ mag}$ (i.e., $T < 7,300\text{ K}$) and most confirmed progenitor stars are red supergiants (as in Smartt 2015). This observation is consistent with

predictions of star formation and stellar evolution, which suggest that SNe from lower mass and redder stars should be more common.

It is therefore of enormous scientific value when SN progenitor stars are detected at the extremes of observed colour and luminosity distributions as these stars can both probe unusual SN explosions found in nature and challenge interpretations of stellar evolution and SN physics. In particular, several SNe IIb (SNe with a strong hydrogen lines at early times that are relatively weak at later times, implying a thin hydrogen envelope) have been discovered with progenitor star detections, which appear to span the stellar temperature range from red to blue supergiants (see, e.g., SN 2013df and SN 2008ax; Van Dyk et al. 2014; Crockett et al. 2008). Examples such as SN 1993J (Aldering et al. 1994) challenge single-star evolution models as their progenitor star colours cannot be matched to the end points of most plausible evolutionary tracks. This discovery has led to the interpretation that at least some SNe IIb come from binary star systems where mass from the progenitor star has been stripped by a companion (Nomoto et al. 1993; Woosley et al. 1994; Fox et al. 2014).

In this paper, we discuss SN 2016gkg discovered in NGC 613. This SN was discovered by Buso & Otero (2016) on 20.18 September (all dates presented herein are UT) and reported in a subsequent detection on 20.54 September by Tonry et al. (2016). Within the

* Email: cdkilpat@ucsc.edu

9 hours between these detections, the SN appeared to have brightened by ~ 3 mag. Jha et al. (2016) reported a spectroscopic confirmation on 21.9 September that SN 2016gkg was a young Type II SN. Subsequent high-resolution spectroscopy on 25.33 September by Andrews & Smith (2016) found broad H α emission with P-Cygni features that matched SN 1987A around peak magnitude. On 28.56 September, Van Dyk et al. (2016) found in low-resolution spectroscopy that SN 2016gkg more closely resembled a SN Iib. Here, we present early-time imaging of SN 2016gkg and a subsequent spectral epoch. We discuss detailed astrometry of the SN at early times, which demonstrate that the position of the SN is consistent with a blue source detected in archival *Hubble Space Telescope* (*HST*) Wide Field Planetary-Camera 2 (WFPC2) imaging. We fit the magnitudes derived from this source to stellar spectra and demonstrate that the best match is an A0Ia star. Based on comparison to single and binary stellar evolution tracks, we show that this star most likely evolved in a binary system. Finally, we analyse the early-time light curve of SN 2016gkg, which rose rapidly in luminosity within a day after discovery, consistent with predictions from the cooling phase of shock break-out. We show that the stellar radius derived from this light curve is consistent with the radius of the detected progenitor star. Throughout this paper, we assume a Tully-Fisher distance to NGC 613 of 26.4 ± 5.3 Mpc, with a corresponding distance modulus of 32.11 ± 0.44 (Nasonova et al. 2011), and Milky Way extinction of $A_V = 0.053$ (Schlafly & Finkbeiner 2011).

2 OBSERVATIONS

2.1 Archival Data

We obtained archival imaging of NGC 613 from the *HST* Legacy Archive¹ from 21 August 2001 (Cycle 10, Proposal ID 9042, PI Stephen Smartt). The *HST*+WFPC2 data consisted of two frames each of F450W, F606W, and F814W totaling 2×160 s per filter. These data had been combined and calibrated by the Canadian Astronomical Data Centre using the latest calibration software and reference files, including corrections for bias, dark current, flat-fielding, and bad pixel masking. The images had been combined using the IRAF² task MULTIDRIZZLE, which performs automatic image registration, cosmic ray rejection, and final image combination using the DRIZZLE task. We performed photometry on these final, calibrated images in each filter using the DOLPHOT³ stellar photometry package. Finally, we combined the images in all three filters using the MULTIDRIZZLE task, weighting each image by the inverse-variance of emission-free regions in order to produce a reference image with the highest signal-to-noise for each point source. This image is shown in Figure 1.

We also obtained post-explosion photometry of SN 2016gkg recorded from Buso & Otero (2016); Nicholls et al. (2016); Tonry et al. (2016); Chen et al. (2016). These data included observations from the All Sky Automated Survey for SuperNovae (ASAS-SN), the Asteroid Terrestrial-impact Last Alert System

Table 1. Ultraviolet/Optical Photometry of SN 2016gkg

UT Date (from 20 September 2016)	Telescope	Filter	Magnitude	Uncertainty	Reference
0.1653	ASAS-SN	V	>17.36	—	(1)
0.2484	Buso & Otero	“clear”	17.6	0.5	(2)
0.54	ATLAS	<i>o</i>	15.94	0.13	(3)
0.55	ATLAS	<i>o</i>	15.78	0.08	(3)
1.1398	Buso & Otero	“clear”	14.5	0.2	(2)
1.2987	ASAS-SN	V	15.01	0.04	(1)
1.6569	Swift	UVW1	13.75	0.04	(4)
1.6588	Swift	U	13.97	0.04	(4)
1.6598	Swift	B	15.21	0.04	(4)
1.6608	Swift	UVW2	13.92	0.04	(4)
1.6645	Swift	V	15.09	0.05	(4)
1.7318	Swift	UVM2	15.28	0.25	(4)
2.1276	LCOGT	B	15.70	0.04	(4)
2.1289	LCOGT	V	15.54	0.03	(4)
2.1302	LCOGT	<i>g</i>	15.61	0.03	(4)
2.1315	LCOGT	<i>i</i>	15.65	0.04	(4)
2.1328	LCOGT	<i>r</i>	15.59	0.04	(4)
2.2884	ASAS-SN	V	15.73	0.05	(4)
2.3946	LCOGT	B	16.01	0.08	(4)
2.3959	LCOGT	V	15.84	0.06	(4)
2.3972	LCOGT	<i>g</i>	15.91	0.07	(4)
2.3998	LCOGT	<i>r</i>	15.85	0.08	(4)

References: (1) Nicholls et al. (2016), (2) Buso & Otero (2016), (3) Tonry et al. (2016), (4) Chen et al. (2016)

(ATLAS), and *Swift*, as well as photometry from the 1-meter telescope on Cerro Tololo, Chile as part of the Las Cumbres Observatory Global Telescope Network (LCOGT). The early-time photometry is summarized in Table 1, which was obtained from Chen et al. (2016).

2.2 Adaptive Optics Imaging

We observed SN 2016gkg in K' band with the Near-Infrared Camera 2 (NIRC2) on the Keck-II 10-m telescope in conjunction with the adaptive optics (AO) system on 22 September 2016, as summarized in Kilpatrick et al. (2016). These data consisted of 30 individual frames each consisting of 3 co-adds of 10 s for an effective exposure time of 30 s per frame and 900 s total. The individual frames were corrected for pixel-to-pixel variations using a flat-field frame that was created from the science frames themselves, and then sky-subtracted. Images taken with NIRC2 have known optical distortions. Therefore, each of the individual frames was resampled to a corrected grid, using the coordinate distortions that are provided on the NIRC2 website⁴. We masked each individual frame in order to remove bad pixels, cosmic-rays, and additional image artifacts. Finally, we aligned the individual frames using an offset vector calculated from the position of the SN and combined the individual frames. In Figure 1, we show the AO imaging along with the reference *HST* archival image.

2.3 Spectroscopy

A spectrum of SN 2016gkg was obtained on 8 October 2016 with the Goodman Spectrograph (Clemens et al. 2004) and the 4.1-m Southern Astrophysical Research Telescope (SOAR) on Cerro Pachón, Chile. We used the $1.07''$ slit in conjunction with the 400 l/mm grating for an effective spectral range of 4000–7050 Å on the blue side and 5000–9050 Å on the red side and a single

¹ https://hla.stsci.edu/hla_faq.html

² IRAF, the Image Reduction and Analysis Facility, is distributed by the National Optical Astronomy Observatory, which is operated by the Association of Universities for Research in Astronomy (AURA) under cooperative agreement with the National Science Foundation (NSF).

³ <http://americano.dolphinsim.com/dolphot/>

⁴ http://www2.keck.hawaii.edu/inst/nirc2/nirc2dewarp_position

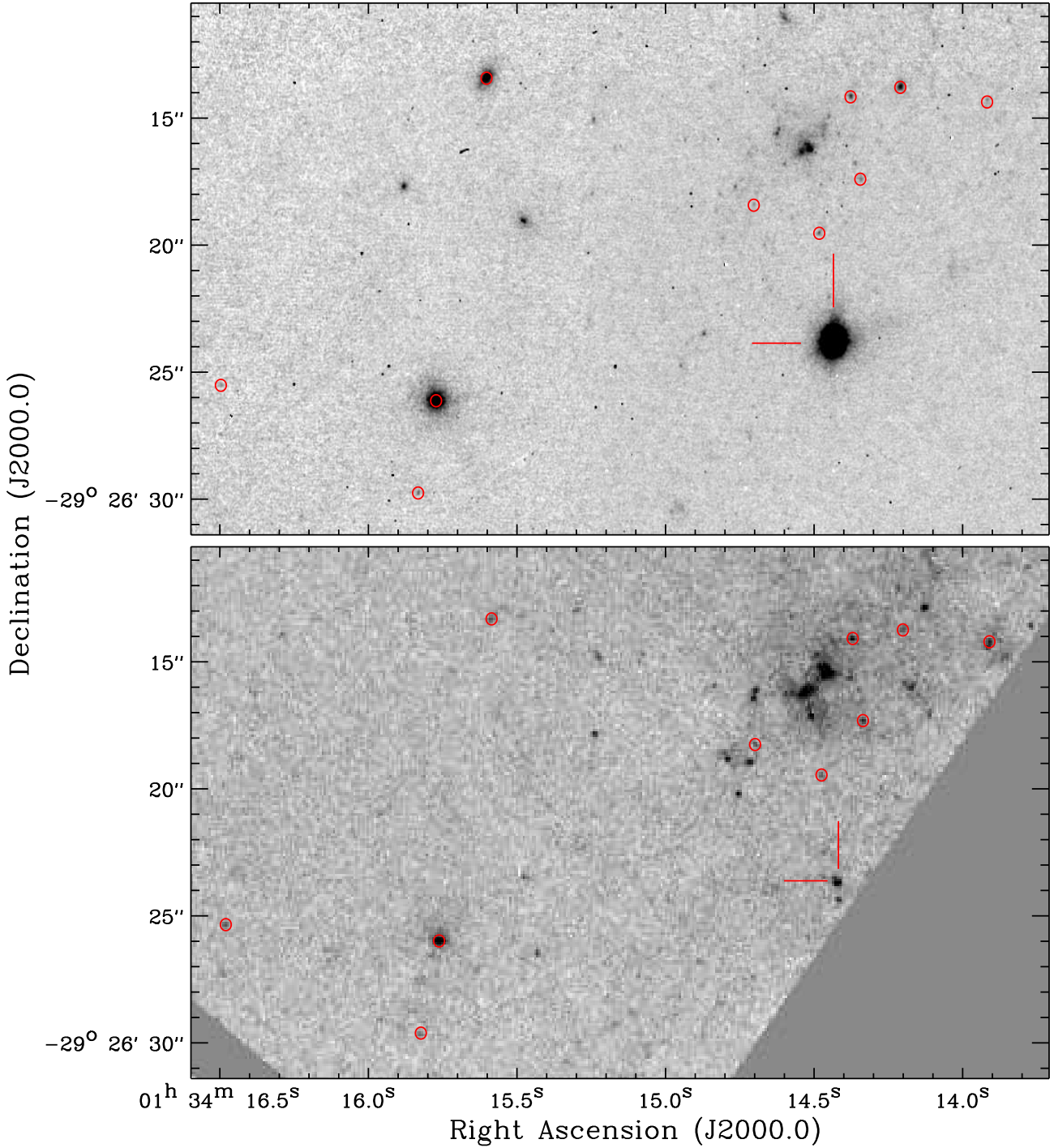


Figure 1. (Upper panel) Keck NIRC2 AO K' imaging of SN 2016gkg. The SN is denoted and 10 point sources used for astrometry are circled in red. (Bottom panel) *HST* WFPC2 F450W+F606W+F814W reference image used for astrometry. The progenitor star is denoted and the same 10 point sources from the NIRC2 image are circled in red.

1200 s exposure per side. A blocking filter (GG-455) was used in the red to minimise second-order scattering of blue light onto the CCD. During our observations, we aligned the slit with the center of NGC 613 in order to simultaneously observe the SN and host galaxy. The SN was at an airmass of ~ 1.01 at this time and chromatic atmospheric dispersion was minimal. Conditions were pho-

tometric at the time of observations with $\sim 0.8''$ seeing. We used IRAF to perform standard reductions on the two-dimensional images and optimal extraction of the one-dimensional blue and red side spectra. We performed wavelength calibration on these one-dimensional images using arc lamp exposures taken immediately after each spectrum. We derived a sensitivity function from a stan-

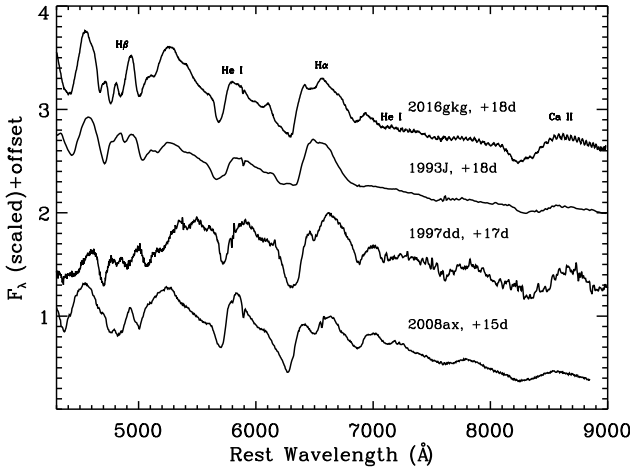


Figure 2. SN 2016gkg spectrum with the day relative to explosion (##d) of observation given in black. For comparison, we also plot the SNe IIB 1993J, 1997dd, and 2008ax at a similar epoch relative to explosion (to discovery for 1997dd; Matheson et al. 2000, 2001; Taubenberger et al. 2011). All spectra have been dereddened and their recession velocities have been removed given the parameters provided in each reference. We indicate prominent emission and absorption features in these SN IIB spectra, including H α , H β , He I $\lambda\lambda$ 5876 and 7065, and the Ca II infrared triplet.

dard star obtained at similar airmass and in the same instrument configuration and used this function to perform flux calibration. We dereddened the spectrum using the extinction quoted above and removed the recession velocity $v = 1,480 \text{ km s}^{-1}$, which is consistent with the velocity of the host galaxy. Finally, we combined the red and blue spectra into a single spectrum, which is presented in Figure 2.

3 RESULTS AND DISCUSSION

3.1 Spectrum of SN 2016gkg

In Figure 2, we compare our spectrum of SN 2016gkg to spectra of the SNe IIB 1993J, 1997dd, and 2008ax (Matheson et al. 2000, 2001; Taubenberger et al. 2011). The comparison spectra have been dereddened and their recession velocities have been removed according to the extinction and redshift information provided in each reference. We indicate the relative epoch of each spectrum with respect to the explosion dates calculated for SNe 2016gkg, 1993J, and 2008ax (see below and Matheson et al. 2000; Taubenberger et al. 2011) and with respect to discovery date on 26.18 Aug 1997 for SN 1997dd (Nakano et al. 1997).

The comparison between these spectra, especially in He I $\lambda\lambda$ 5876 and 7065 absorption, strongly suggests that SN 2016gkg is a SN IIB and was around or slightly before peak magnitude (or secondary peak as in SN 1993J; Benson et al. 1994). The development of these He I features appears to be more rapid than in SN 1993J based on our estimated explosion date for SN 2016gkg (Section 3.5) and is more similar to SN 2008ax at this epoch. In addition, H α is not a dominant emission feature in SN 2016gkg at this epoch, implying that the initial hydrogen emission may be fading relative to the continuum level. Our spectrum is very similar to the early spectrum of SN 1997dd, where a distinct “notch” developed in the H α line, likely due to the P-Cygni profile of He I λ 6678 before He absorption had fully developed (e.g., Matheson et al.

2001). We note additional similarities to SN 1997dd, which was identified early as a peculiar Type II SN with weak H α emission (Suntzeff & Phillips 1997), as with SN 2016gkg in analysis by Jha et al. (2016).

As we mention in Section 2, we aligned the slit of the Goodman Spectrograph to obtain a spectrum of NGC 613 simultaneously with SN 2016gkg. Analysis of the host galaxy emission line ratio

$$\log R_{23} = \frac{I_{[\text{O II}]\lambda 3727} + I_{[\text{O III}]\lambda 4959} + I_{[\text{O III}]\lambda 5007}}{I_{\text{H}\beta}} \quad (1)$$

using the calibration in Kobulnicky & Kewley (2004) suggests that NGC 613 has $12 + \log(\text{O}/\text{H}) = 8.61 \pm 0.15$ with an implied metallicity of $Z = 0.012 \pm 0.004$. This value is slightly sub-solar ($12 + \log(\text{O}/\text{H})_{\odot} = 8.7$), although it agrees with the solar value to within our error bars. We adopt $Z = 0.012$ for subsequent analysis of the SN 2016gkg progenitor star.

3.2 Astrometry of the AO Imaging and HST Point Source

We performed relative astrometry on the AO image and composite *HST* image using the 10 common sources circled in both frames (Figure 1). The positions derived for these 10 sources were determined using DOLPHOT in each frame and image registration was carried out on the AO image using the IRAF tasks CCMAP and CCSETWCS. The astrometric uncertainty was $\sigma_{\alpha} = 0.023''$, $\sigma_{\delta} = 0.036''$. The position of the progenitor star in the *HST* reference image is $\alpha = 1^{\text{h}}34^{\text{m}}14^{\text{s}}.418$, $\delta = -29^{\circ}26'23''.83$ and is detected with $\text{S/N} = 5.8$ for an astrometric precision of $0.052''$. Relative astrometry from the AO image suggests that the position of SN 2016gkg is $\alpha = 1^{\text{h}}34^{\text{m}}14^{\text{s}}.424$, $\delta = -29^{\circ}26'23''.82$ for an offset of $\Delta\alpha = +0.05''$, $\Delta\delta = -0.01''$. The combined offset is well within the uncertainty from *HST* astrometry and relative astrometry (0.89σ ; astrometric uncertainty from the position of SN 2016gkg is negligible), and we conclude that the positions of these objects agree with each other. This evidence strongly suggests that the point source detected in archival *HST* imaging is the progenitor star of SN 2016gkg.

We estimate the probability of a chance coincidence in the *HST* image by noting that there are a total of 12 point sources with $\text{S/N} > 3$ in the *HST* image from Figure 1. The 3σ error ellipse for the *HST* reference image has a solid angle of approximately 0.64 arcsec^2 , which implies that $\sim 7.6 \text{ arcsec}^2$ or 0.12% of the *HST* archival image has a point source that is close enough to be associated with that region. This value represents the probability that the detected point source is a chance coincidence, and we find that it is extremely unlikely that the blue point source was aligned with the position of the SN by chance.

3.3 Photometric Classification of the Progenitor Star

From our photometric analysis of the SN 2016gkg progenitor star, we obtained ST magnitudes $m_{\text{F450W}} = 22.93 \pm 0.47$, $m_{\text{F606W}} = 23.40 \pm 0.33$, $m_{\text{F814W}} = 24.56 \pm 0.59 \text{ mag}$. We corrected these values for interstellar extinction using Equations (3a), (3b), (4a), and (4b) in Cardelli et al. (1989) with $R_V = 3.1$, which we use for all photometry herein.

We used these magnitudes to determine the spectral type of the SN 2016gkg progenitor star using stellar spectra from Pickles (1998). Fitting the redshift-corrected flux density to stellar spectra convolved with the WFPC2 transmission curves for the F450W, F606W, and F814W filters, we determined the best-fitting stellar

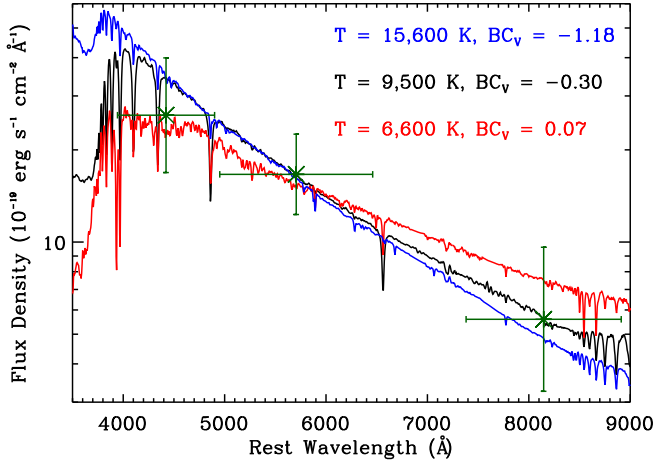


Figure 3. *HST* archival photometry from the SN 2016gkg progenitor star. The wavelength uncertainty of each point represents the width of the corresponding WFC2 filter. Each point has been corrected for extinction and the recessional velocity of NGC 613 has been removed from the effective wavelength. Overplotted are the best-fit (black) and $\Delta\chi^2/\chi^2_{\min} = 1$ (red/blue) stellar spectra obtained from Pickles (1998). We indicate the temperature and bolometric correction of each stellar spectrum in the upper-right of the panel.

spectrum and thus the temperature and bolometric correction by minimising the χ^2 of the observed and model flux densities. In Figure 3, we show the best-fitting stellar spectrum in black along with the stellar spectra with the lowest (red) and highest (blue) implied temperatures that were within $\Delta\chi^2/\chi^2_{\min} = 1$ of the minimum χ^2 . The implied best-fitting temperature and bolometric correction are $T = 9500^{+6100}_{-2900}$ K and $BC_V = -0.30^{+0.37}_{-0.88}$ mag. These values correspond to a spectral class of A0.

From the best-fitting stellar spectra, the implied flux density in Johnson *V* band is $7.2^{+3.2}_{-2.3} \times 10^{-19}$ erg s $^{-1}$ cm $^{-2}$ Å $^{-1}$ or $m_V = 24.3 \pm 0.4$ mag (implying the best-fitting stellar type is A0Ia), which suggests that the overall bolometric magnitude is $m_{\text{bol}} = 24.0^{+0.54}_{-0.97}$ mag. The luminosity of the SN 2016gkg progenitor star is therefore $\log(L/L_{\odot}) = 5.14^{+0.22}_{-0.39}$ with an implied radius of $\log(R/R_{\odot}) = 2.14^{+0.29}_{-0.59}$. We note that these values are remarkably similar to the progenitor star model for SN 2008ax in Crockett et al. (2008) where the authors found the photometry was well-fit by a B8 to early K supergiant combined with a M4 supergiant, the former having $\log(L/L_{\odot}) = 5.1$, $T = 8900$ K (see also Smartt 2015). In our discussion of the SN 2016gkg spectrum above, we emphasize this comparison with SN 2008ax at 15 days after explosion.

3.4 Matching the SN 2016gkg to Stellar Evolution Tracks

In order to constrain the zero-age main-sequence mass (M_{ZAMS}) and evolutionary path of a SN progenitor star, it is necessary to compare the luminosity and temperature derived from photometry to model evolutionary tracks. This analysis has been done for a number of SNe I Ib including SN 1993J (Podsiadlowski 1993), SN 2008ax (Crockett et al. 2008), SN 2011dh (Maund et al. 2011; Van Dyk et al. 2011; Bersten et al. 2012), and SN 2013df (Van Dyk et al. 2014). Here, we analyse the temperature and luminosity derived for SN 2016gkg to single- and binary-star models

on the Hertzsprung-Russell (HR) diagram and make comparisons to these example SN I Ib progenitor stars.

3.4.1 Single-Star Models

Single-star models were obtained from Brott et al. (2011) for $M_{\text{ZAMS}} = 5 - 60 M_{\odot}$ stars. We examined models with metallicity $Z = 0.0088$, which was the closest set to the observed metallicity of NGC 613. We overplot these models with the observed parameters of the SN 2016gkg progenitor star on the HR diagram in Figure 4. As we demonstrate, there are no single-star models that are consistent with ending their evolutionary tracks near the predicted luminosity and temperature values.

We find that it is extremely unlikely that SN 2016gkg originated from a single-star, even accepting moderately inflated uncertainties such that the SN 2016gkg progenitor star is consistent with stars with $M_{\text{ZAMS}} \sim 40\text{--}50 M_{\odot}$. Woosley & Heger (2007) and Sukhbold et al. (2016) have found that, for stars with $M_{\text{ZAMS}} > 30 M_{\odot}$, the pre-supernova iron core is too large for a SN to be successful. Moreover, mass loss is sufficiently strong that most of these stars lose their entire hydrogen envelopes and are thought to end their evolution as Wolf Rayet stars, implying that the subsequent SN would be Type Ib or Ic. SNe I Ib require progenitor stars with extended low-mass hydrogen envelopes (Podsiadlowski 1993; Woosley et al. 1994; Elmhamdi et al. 2006), and any single-star model for such a system would require finely tuned mass loss that would otherwise fail to reproduce the observed range in SN I Ib light curves, spectra, and progenitor stars. While the single-star scenario could describe a minority of SNe I Ib, it is likely that the majority of these systems come from binary-star systems such as the one observed toward SN 1993J (Maund et al. 2004; Fox et al. 2014).

3.4.2 Binary-Star Models

We examine evolutionary tracks involving binary stars in order to assess the plausibility of these systems as possible progenitor stars for SN 2016gkg. We obtained our binary star evolutionary tracks from the Binary Population and Spectral Synthesis (BPASS) code as described in (Eldridge & Stanway 2009). These models provide a range of metallicities ($Z = 0.001\text{--}0.040$), primary star masses ($M/M_{\odot} = 0.1\text{--}300$), mass ratios ($q = 0.1\text{--}0.9$), and initial periods ($\log(P/1 \text{ day}) = 0\text{--}4$). We fixed the metallicity of the binary-star models to $Z = 0.010$ in order to provide the best match to the observed metallicity of NGC 613. Otherwise, we examined the full range of parameters provided by BPASS.

For our fitting scheme, we looked for binary-star models that produced a primary star with terminal luminosity and temperature that matched those observed for the SN 2016gkg progenitor star. Overall, we found 107 out of 5565 BPASS models with primary star parameters in this allowed range. In Figure 4, we show the stellar evolution of the best-fitting binary-star model on the HR diagram along with the inferred luminosity and temperature of the SN 2016gkg progenitor star. The primary star has an initial mass of $15 M_{\odot}$ while the secondary (accreting) star has an initial mass of $1.5 M_{\odot}$ and an initial orbital period of 1000 days. We note in Figure 4 that the pre-explosion mass of the best-fitting star is $M = 5.2 M_{\odot}$. The hydrogen that remains in the envelope from this best-fitting model is $5 \times 10^{-3} M_{\odot}$, which agrees with models of SNe I Ib (Dessart et al. 2011).

If SN 2016gkg evolved from a binary-star system, it may be

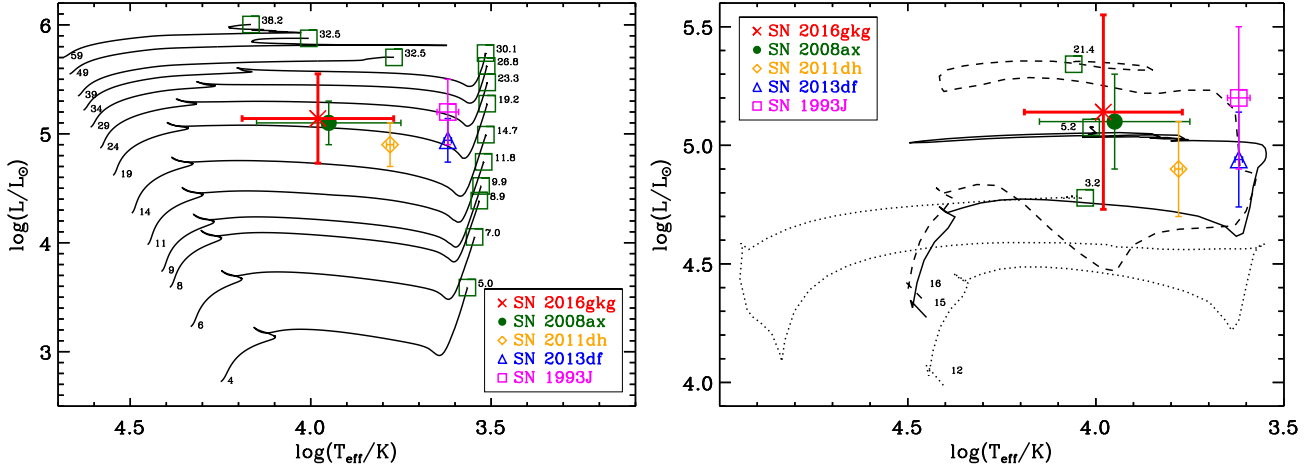


Figure 4. (Left) Single-star evolutionary tracks plotted on the HR diagram with the inferred luminosity and temperature from SN 2016gkg overplotted. We also indicate the inferred luminosities and temperatures from the SNe IIB 2008ax, 2011dh, 2013df, and 1993J (Crockett et al. 2008; Maund et al. 2011; Van Dyk et al. 2011, 2014; Aldering et al. 1994). The initial mass and final mass of the modeled star are given near the start and end points of each evolutionary track (the latter is indicated with a square). As we demonstrate, no single-star evolutionary track terminates near the inferred luminosity and temperature of the SN 2016gkg — or any other SN IIB — progenitor star. (Right) Same as the left but for the binary star models that terminate at values in agreement with the inferred luminosity and temperature for SN 2016gkg (as discussed in Section 3.4.2). The best-fitting model has an initial stellar mass of $M = 15 M_{\odot}$ with a $1.5 M_{\odot}$ companion. The initial period is 1000 days and the primary star explodes with $M = 5.2 M_{\odot}$. Two additional examples with initial masses $12 M_{\odot}$ ($8.4 M_{\odot}$ initial mass companion, 160 day period) and $16 M_{\odot}$ ($14.4 M_{\odot}$ initial mass companion, 6.3 day period) are shown with dotted and dashed lines, respectively. All of these models agree with the inferred luminosity and temperature of SN 2016gkg.

possible to detect the companion star in follow-up photometry after the SN has faded. The secondary star in our best-fitting binary star model is intrinsically much fainter than the SN 2016gkg progenitor star. Accounting for distance modulus and extinction, its expected brightness in F300W is 25.9 mag. It may be feasible to search for such a companion with sufficiently deep imaging.

3.5 Modeling the Early-Time Light Curve of SN 2016gkg

The early-time light curve of any SN can yield important information about the progenitor star when shock break-out is observed. For SNe other than SNe II-P, observations of this phase are extremely scarce as their progenitor stars are thought to have less extended envelopes which implies a fast rise and decline in the early-time light curve. In the rare cases where this phase is observed, hydrodynamical models can constrain the radius of the progenitor star, as larger stars tend to have hotter effective temperatures with a more luminous initial peak while smaller stars tend to appear cooler. In our analysis of the early-time light curve, we use models derived from Rabinak & Waxman (2011) for a star with a hydrogen envelope density profile $\rho \approx (1 - r/R_*)^3$ (where R_* is the stellar radius). In general, we assume that the progenitor star has a blackbody color temperature 20% larger than the photospheric temperature and typical Thomson scattering opacity $\kappa = 0.34 \text{ cm}^2 \text{ g}^{-1}$. Rabinak & Waxman (2011) and Bersten et al. (2012) demonstrated that these assumptions are good approximations of more detailed models for $t < 1$ day after explosion.

In order to calculate the radius of the progenitor star, we must make assumptions about the explosion energy and ejecta mass of SN 2016gkg. These parameters are well-known for the SN IIB 1993J, which we have demonstrated is a good match for SN 2016gkg at the epoch of our spectroscopic observation. We employ parameters for a SN 1993J-like explosion with ejecta mass, $M_{\text{ej}} = 2.6 M_{\odot}$, and explosion energy, $E = 10^{51} \text{ erg}$ (Woosley et al. 1994; Young et al. 1995). Using these parameters,

we fit specific luminosity to the model at a time t since explosion with

$$L_{\lambda} = 0.234 \mu r^2 \frac{(hc/\lambda)^5}{\exp(hc/\lambda T) - 1} \quad (2)$$

$$r = 3.3 \times 10^{14} \frac{E_{51}^{0.39} \kappa_{0.34}^{0.11}}{(M_{\text{ej}}/M_{\odot})^{(0.28)}} t_5^{0.78} \text{ cm} \quad (3)$$

$$T = 1.6 \frac{E_{51}^{0.016} R_{*,13}^{1/4}}{(M_{\text{ej}}/M_{\odot})^{0.033} \kappa_{0.34}^{0.27}} t_5^{-0.47} \text{ eV} \quad (4)$$

where $E = E_{51} 10^{51} \text{ erg}$, $\kappa = \kappa_{0.34} 0.34 \text{ cm}^2 \text{ g}^{-1}$, $t = t_5 10^5 \text{ s}$, $R_* = R_{*,13} 10^{13} \text{ cm}$, and $\mu = 1.14 \times 10^{12} \text{ cm}^{-3} \text{ s}^{-1} \text{ K}^{-4}$ (i.e., the ratio of the radiation constant to the Planck constant). As we have noted, this model breaks down for times significantly (e.g., > 1 day) after explosion. Therefore, in determining the explosion date and stellar radius, we fit only photometry within 1.5 days of the ASAS-SN V band limit on 20.165 September 2016. These include the discovery magnitudes and followup photometry from Nicholls et al. (2016) and Tonry et al. (2016).

We constructed a range of models using the equations above and convolved the specific luminosity with the filter transmission curves. In Figure 5, we show our best-fitting model for a range of filters, including ASAS-SN V , ATLAS o , the “clear” filter, and the *Swift* UVW2. Our best-fitting model corresponds to a stellar radius of $\log(R/R_{\odot}) = 2.41^{+0.40}_{-0.58}$ and an explosion date of $t_0 = 20.15^{+0.08}_{-0.10}$ September 2016. Our range of best-fitting parameters is also displayed in Figure 5 with contours representing χ^2 overplotted.

The early-time light curve agrees with all of the photometry within 1.5 days of explosion to within the $1\text{-}\sigma$ uncertainties. After this point, there is general disagreement between the model and observed magnitudes, especially at redder wavelengths where the model overpredicts the specific luminosities and does not turn over as quickly as the observed light curve. This disagreement is likely

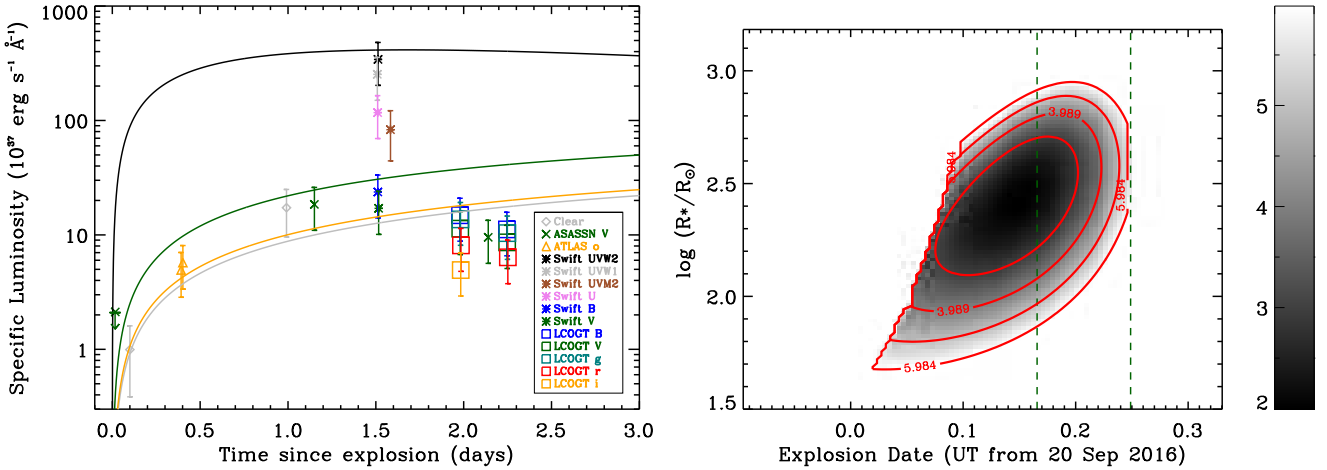


Figure 5. (Left) Early-time light curve of SN 2016gkg as discussed in Section 3.5 and referenced in Nicholls et al. (2016) and Tonry et al. (2016). The data are plotted in terms of specific luminosity (i.e., $L_\lambda = 4\pi D^2 f_\lambda$). Overplotted are light curves of the cooling phase that follows shock break-out based on models provided in Rabinak & Waxman (2011) and for a range of filter transmission curves including “clear” (grey), ATLAS o (orange), ASAS-SN V (green), and Swift UVW2 (black). These models use the best-fitting explosion time and progenitor star radius derived from photometry within 1.5 days of the initial ASAS-SN V band upper limit (indicated on the left with an arrow). Other parameters used to derive these light curves are described in Section 3.5. (Right) χ^2 for the range of model parameters used to derive the light curves on the left. We have overplotted two dashed lines to indicate the time of the ASAS-SN V band upper-limit (20.1653 September 2016) and the first photometry point (20.2484 September 2016), which place the strongest constraints on the explosion date.

caused by our assumption of a constant Thomson-like opacity, independent of time and spatial coordinate in the model star. In more realistic models, the opacity is sensitive to the ionisation state of the model star and decreases as hydrogen in the envelope recombines. However, good agreement can be found at early times between this model and the SN 1987A light curve (Rabinak & Waxman 2011) and the SN 2011dh light curve (Bersten et al. 2012) where most of the hydrogen envelope is ionised. Therefore, we are confident that the explosion date and progenitor star radius inferred from this model is an accurate representation of the light curve.

4 CONCLUSIONS

We describe new astrometric and photometric analysis of the SN 2016gkg progenitor star as well as optical photometry and spectroscopy of the SN itself. Our analysis yields new insight into SN 2016gkg and we find the following:

(i) Astrometric analysis of our AO imaging indicates the SN position is consistent with the position of a blue point source in *HST* imaging. Fitting the photometry of this source, we find the best-fitting stellar model to be an A0Ia star with $\log(L/L_\odot) = 5.14^{+0.22}_{-0.39}$ and $T = 9500^{+6100}_{-2900}$ K and implied radius of $\log(R/R_\odot) = 2.14^{+0.29}_{-0.59}$.

(ii) Based on the best-fitting luminosity and temperature of the SN 2016gkg progenitor star, we find that single-star models do not terminate with the inferred properties. Rather, we find that binary-star models are required to produce evolutionary tracks with primary star terminal properties that match the SN 2016gkg progenitor star. The best-fitting binary-star model involves a primary star with $M_{\text{ZAMS}} = 15 M_\odot$ and a secondary with $M_{\text{ZAMS}} = 1.5 M_\odot$. With sufficiently deep imaging, it may be possible to detect the secondary star once the SN has faded significantly.

(iii) We fit analytic models of the cooling phase that follows shock break-out to the specific luminosity observed from SN 2016gkg. These models are sensitive to both the explosion date

and radius of the progenitor star. Our best-fitting explosion date and progenitor star radius are $t_0 = 20.15^{+0.08}_{-0.10}$ September 2016 and $\log(R/R_\odot) = 2.41^{+0.40}_{-0.58}$. The latter value is in agreement with the radius fit to the progenitor star from pre-explosion photometry.

ACKNOWLEDGMENTS

We would like to thank John Tonry for providing data from ATLAS, as well as Dan Kasen, Josiah Schwab, Enrico Ramirez-Ruiz, and Stan Woosley for their helpful discussions. We also thank Marc Kassiss for his assistance with Keck data acquisition and Nathan Smith and Jennifer Andrews for discussing spectroscopy of SN 2016gkg.

The UCSC group is supported in part by NSF grant AST-1518052 and from fellowships from the Alfred P. Sloan Foundation and the David and Lucile Packard Foundation to R.J.F.

Some of the data presented herein were obtained at the W. M. Keck Observatory, which is operated as a scientific partnership among the California Institute of Technology, the University of California, and NASA. The observatory was made possible by the generous financial support of the W. M. Keck Foundation. We wish to recognise and acknowledge the cultural significance that the summit of Mauna Kea has within the indigenous Hawaiian community. We are most fortunate to have the opportunity to conduct observations from this mountain.

Some of our photometry of SN 2016gkg comes from All Sky Automated Survey for SuperNovae (ASAS-SN), the Asteroid Terrestrial-impact Last Alert System (ATLAS), *Swift*, and the Las Cumbres Observatory Global Telescope Network (LCOGT). The *Hubble Space Telescope* (*HST*) is operated by NASA/ESA. Some of our analysis is based on data obtained from the *HST* archive operated by STScI. Our analysis is based in part on observations obtained at the Southern Astrophysical Research (SOAR) telescope, which is a joint project of the Ministério da Ciência, Tecnologia, e Inovação (MCTI) da República Federativa do Brasil, the U.S. National Optical Astronomy Observatory (NOAO), the University of North Carolina at Chapel Hill (UNC), and Michigan State University (MSU).

Facilities: Keck (NIRC2), SOAR (Goodman)

REFERENCES

Aldering G., Humphreys R. M., Richmond M., 1994, *AJ*, **107**, 662

- Andrews J., Smith N., 2016, The Astronomer’s Telegram, [9562](#)
- Arnett W. D., 1987, [ApJ](#), **319**, [136](#)
- Arnett W. D., Bahcall J. N., Kirshner R. P., Woosley S. E., 1989, [ARA&A](#), **27**, [629](#)
- Benson P. J., et al., 1994, [AJ](#), **107**, [1453](#)
- Bersten M. C., et al., 2012, [ApJ](#), **757**, [31](#)
- Brott I., et al., 2011, [A&A](#), **530**, [A115](#)
- Buso V., Otero S., 2016, vsnet-alert 20188
- Cardelli J. A., Clayton G. C., Mathis J. S., 1989, [ApJ](#), **345**, [245](#)
- Chen P., et al., 2016, The Astronomer’s Telegram, [9529](#)
- Clemens J. C., Crain J. A., Anderson R., 2004, in Moorwood A. F. M., Iye M., eds, Proc. SPIE Vol. 5492, Ground-based Instrumentation for Astronomy. pp 331–340, [doi:10.1117/12.550069](#)
- Crockett R. M., et al., 2008, [MNRAS](#), **391**, [L5](#)
- Dessart L., Hillier D. J., Livne E., Yoon S.-C., Woosley S., Waldman R., Langer N., 2011, [MNRAS](#), **414**, [2985](#)
- Eldridge J. J., Stanway E. R., 2009, [MNRAS](#), **400**, [1019](#)
- Elmhamdi A., Danziger I. J., Branch D., Leibundgut B., Baron E., Kirshner R. P., 2006, [A&A](#), **450**, [305](#)
- Fox O. D., et al., 2014, [ApJ](#), **790**, [17](#)
- Jha S. W., Van Wyk V., Vaisanen P., 2016, The Astronomer’s Telegram, [9528](#)
- Kilpatrick C. D., et al., 2016, The Astronomer’s Telegram, [9536](#)
- Kobulnicky H. A., Kewley L. J., 2004, [ApJ](#), **617**, [240](#)
- Matheson T., et al., 2000, [AJ](#), **120**, [1487](#)
- Matheson T., Filippenko A. V., Li W., Leonard D. C., Shields J. C., 2001, [AJ](#), **121**, [1648](#)
- Mauerhan J. C., et al., 2013, [MNRAS](#), **430**, [1801](#)
- Maund J. R., Smartt S. J., Kudritzki R. P., Podsiadlowski P., Gilmore G. F., 2004, *Nature*, **427**, [129](#)
- Maund J. R., et al., 2011, [ApJ](#), **739**, [L37](#)
- Morris T., Podsiadlowski P., 2007, *Science*, **315**, [1103](#)
- Nakano S., Aoki M., Garnavich P., Kirshner R., Stanek K., 1997, *IAU Circ.*, **6724**
- Nasonova O. G., de Freitas Pacheco J. A., Karachentsev I. D., 2011, [A&A](#), **532**, [A104](#)
- Nicholls B., et al., 2016, The Astronomer’s Telegram, [9521](#)
- Nomoto K., Suzuki T., Shigeyama T., Kumagai S., Yamaoka H., Saio H., 1993, *Nature*, **364**, [507](#)
- Pickles A. J., 1998, *PASP*, **110**, [863](#)
- Podsiadlowski P., 1993, *Space Sci. Rev.*, **66**, [439](#)
- Rabinak I., Waxman E., 2011, [ApJ](#), **728**, [63](#)
- Schlafly E. F., Finkbeiner D. P., 2011, [ApJ](#), **737**, [103](#)
- Smartt S. J., 2015, *Publ. Astron. Soc. Australia*, **32**, [e016](#)
- Smartt S. J., Eldridge J. J., Crockett R. M., Maund J. R., 2009, [MNRAS](#), **395**, [1409](#)
- Sukhbold T., Ertl T., Woosley S. E., Brown J. M., Janka H.-T., 2016, [ApJ](#), **821**, [38](#)
- Suntzeff N., Phillips M., 1997, *IAU Circ.*, **6725**
- Taubenberger S., et al., 2011, [MNRAS](#), **413**, [2140](#)
- Tonry J., Denneau L., Stalder B., Heinze A., Sherstyuk A., Rest A., Smith K. W., Smartt S. J., 2016, The Astronomer’s Telegram, [9526](#)
- Van Dyk S. D., et al., 2011, [ApJ](#), **741**, [L28](#)
- Van Dyk S. D., et al., 2014, [AJ](#), **147**, [37](#)
- Van Dyk S. D., Zheng W., Shivvers I., Filippenko A. V., Tucker B. E., Perley D. A., Smith N., 2016, The Astronomer’s Telegram, [9573](#)
- Weiler K. W., Williams C. L., Panagia N., Stockdale C. J., Kelley M. T., Sramek R. A., Van Dyk S. D., Marcaide J. M., 2007, [ApJ](#), **671**, [1959](#)
- Woosley S. E., Heger A., 2007, *Phys. Rep.*, **442**, [269](#)
- Woosley S. E., Pinto P. A., Martin P. G., Weaver T. A., 1987, [ApJ](#), **318**, [664](#)
- Woosley S. E., Eastman R. G., Weaver T. A., Pinto P. A., 1994, [ApJ](#), **429**, [300](#)
- Young T. R., Baron E., Branch D., 1995, [ApJ](#), **449**, [L51](#)